*Neuroscience* 140 (2006) 491–504

# ANALYSIS OF BEHAVIOR-RELATED EXCITATORY INPUTS TO A CENTRAL PACEMAKER NUCLEUS IN A WEAKLY ELECTRIC FISH

**S. CURTI, V. COMAS,[1] C. RIVERO[1] AND M. BORDE***

*Dpto. de Fisiología, Laboratorio de Neurofisiología Celular, Facultad de Medicina and Facultad de Ciencias, Gral. Flores 2125, CP 11800, Montevideo, Uruguay*

**Abstract—Gymnotid electric fish explore their environment and communicate with conspecifics by means of rhythmic electric organ discharges. The neural command for each electric organ discharge arises from activity of a medullary pacemaker nucleus composed of two neuronal types: pacemaker and relay cells. During different behaviors as in courtship, exploration and agonistic interactions, these species display specific electric organ discharge frequency and/or waveform modulations. The neural bases of these modulations have been explained in terms of segregation of inputs to pacemaker or relay cells, as well as differential activation of the glutamate receptors of these cells. One of the most conspicuous electric organ discharge frequency modulations in *Gymnotus carapo* results from the activation of Mauthner cells, a pair of reticulospinal neurons that are involved in the organization of sensory-evoked escape responses in teleost fish. The activation of Mauthner cells in these animals produces a prolonged increase in electric organ discharge rate, whose neural mechanisms involves the activation of both *N*-methyl-D-aspartate (NMDA) and metabotropic glutamatergic receptors of pacemaker cells. Here we provide evidence which indicates that pacemaker cells are the only cellular target of the synaptic inputs responsible for the Mauthner cell initiated electric organ discharge modulation at the medullary pacemaker nucleus. Additionally, although pacemaker cells express both NMDA and non-NMDA ionotropic receptors, we found that non-NMDA receptors are not involved in this synaptic action which suggests that NMDA and non-NMDA receptor subtypes are not co-localized at the subsynaptic membrane. NMDA receptor activation of pacemaker cells seems to be an efficient neural strategy to produce long-lasting enhancements of the fish sampling capability during Mauthner cell-initiated motor behaviors. © 2006 Published by Elsevier Ltd on behalf of IBRO.**

**Key words: glutamate receptors, pacemaker, Mauthner cell, electric fish, escape response, NMDA receptors.**

The electrosensory system of weakly electric fish allows them to locate objects and prey in their environment, as well as to communicate with conspecifics (for a review see Hagedorn, 1986; Lorenzo et al., 2001). By means of a highly specialized electromotor system, these species emit rhythmic electric organ discharges (EOD) that are sensed by electroreceptors located in the fish skin (Lissman, 1958; Black-Cleworth, 1970; Hagedorn, 1986). Each EOD is generated by an electric organ in response to a command discharge of a medullary structure, the pacemaker nucleus (PMn) (Szabo, 1957; Bennett, 1971; Dye and Meyer, 1986; Heiligenberg, 1991; Caputi and Aguilera, 1996). The PMn is composed of two different neuronal types: intrinsic pacemaker (PM) cells and projecting relay neurons (Bennett et al., 1967). In gymnotiform fish, the rhythmic command for the EOD is initiated at the PM cells and then transmitted 1:1 to relay cells (for a review see Lorenzo et al., 2001).

Because of its relative anatomical and functional simplicity, the electromotor system has been considered as a model system for studying the neural basis of vertebrate behavior (Heiligenberg, 1991). During various behaviors (exploration, courtship and agonistic interactions), the PMn produces specific output patterns in response to modulatory inputs arising from different prepacemaker structures (Kawasaki et al., 1988; Keller et al., 1991). The basic mechanisms of these synaptic inputs that result in modulations of EOD frequency and/or waveform have been studied in several electric fish species (Dye et al., 1989; Kawasaki and Heiligenberg, 1989, 1990; Spiro, 1997; Juranek and Metzner, 1998). These studies have shown that separate inputs to PM and relay cells as well as activation of different neurotransmitter receptors in these two cell types, result in the production of diverse output patterns that emerge from a simple neural circuit.

The understanding of the neural mechanisms that operate at the PMn during EOD modulations has been facilitated by the analysis of the electromotor behavior triggered by a single action potential in an identified central neuron. Such electromotor behavior is the Mauthner cell (M-cell)-initiated electromotor behavior (M-AIR, from Mauthner-initiated abrupt increase in rate), which has been described in *Gymnotus carapo* (Falconi et al., 1995). This electromotor behavior consists of an abrupt and prolonged acceleration of the EOD, probably associated with an increase in the electrolocative ability of the fish. Intracellular recordings obtained from PM and relay cells during M-AIR suggested that synaptic excitatory effects responsible for this EOD modulation are restricted to PM cells (Falconi et al., 1997). More recently, studying the effects of glutamate antagonists on the electromotor behavior, Curti et al. (1999) concluded that M-AIR most likely results from activation of *N*-methyl-D-aspartate (NMDA) and metabotropic glutamate receptors of PM cells. Strikingly, although

[1] These authors equally contributed to this work.

*Corresponding author. Tel: +598-2-924-7018; fax: +598-2-924-8784.
E-mail address: mborde@fmed.edu.uy (M. Borde).

*Abbreviations:* AP5, (α)-2-amino-5-phosphonopentanoic acid; CNQX, 6-cyano-7-nitroquinoxaline-2,3-dione; CRN, cranial relay neuron; EHP, extrinsic hyperpolarizing potential; ENEP, early negative evoked potential; EOD, electric organ discharge; LNEP, late negative evoked potential; M-AIR, Mauthner-initiated abrupt increase in rate; M-cell, Mauthner cell; NMDA, *N*-methyl-D-aspartate; PM cell, pacemaker cell; PMn, pacemaker nucleus; PSB, Pontamine Sky Blue.

0306-4522/06$30.00+0.00 © 2006 Published by Elsevier Ltd on behalf of IBRO.
doi:10.1016/j.neuroscience.2006.02.037

NMDA and non-NMDA ionotropic glutamate receptors are functionally expressed in this cellular type (Curti et al., 1999), non-NMDA receptors are not apparently involved.

In this paper the neural basis of M-AIR was further investigated *in vivo* by means of a combination of electrophysiological, pharmacological and morphological techniques. Here we provide evidence indicating that PM cells are the only targets of excitatory synaptic inputs underlying the M-AIR at the PMn. These synaptic inputs were recorded extracellularly as a slow- and long-lasting negative potential. The effects induced by specific glutamate receptor antagonists on this potential demonstrate that non-NMDA ionotropic glutamate receptors of PM cells do not participate in the M-cell-initiated electromotor behavior.

## EXPERIMENTAL PROCEDURES

Thirty-five specimens of *Gymnotus carapo* (9–18 cm in length) were used in the present study. The fish were collected in a lake in S.E. Uruguay (Laguna del Sauce, Maldonado) and kept in fresh water aquaria at 20–25 °C. Surgical, recording and stimulation procedures were previously described in detail in Falconi et al. (1995, 1997). Briefly, fish were anesthetized by immersion in iced water. All surgical areas and fixation points were infiltrated with lidocaine. During surgical procedures, the gills were perfused with aerated iced tap water. Paravertebral muscles were removed from one side at a point about 80% down the length of the fish and a bipolar stimulating electrode was placed in contact with the vertebral column to activate the Mauthner axons (Fig. 1); the dorsal surface of the brain was exposed through an opening in the skull to provide access for recording electrodes. Following these procedures, the animals were injected with *d*-tubocurarine (1–3 $\mu$g/g, i.m.) at doses that produced paralysis but did not completely eliminate the EOD. After surgical preparation and curarization, the gills were continuously perfused with aerated tap water at room temperature (20–25 °C). All of these procedures are in accord with the guidelines of the Comisión Honoraria de Experimentación Animal (CHEA), Universidad de la República, Uruguay, and conformed to the international guidelines on the ethical use of animals. All efforts were made to minimize animal suffering and to reduce the number of animals used.

For extracellular recordings, 3 M NaCl-filled micropipettes were used with resistances ranging from 2 to 10 MΩ (Fig. 1). Routinely, field potentials recording were obtained at different depths from the PMn in the ventral medulla and, in selected experiments, also from the vicinity of the left M-cell soma. At the PMn, electrodes were lowered along a vertical line passing near the center of the nucleus. Two successive negative-going potentials were observed at central recording positions (see for an example Fig. 2 A). The recording site at which the first negative potential amplitude reached its maximum and exceeded, or at least was similar to, the amplitude of the late negative potential, was taken as a reference position and will be herein referred to as level 0 $\mu$m. Recordings were conducted at known distances from this level either dorsally (+100 $\mu$m, +200 $\mu$m, etc.) or ventrally (−100 $\mu$m, −200 $\mu$m, etc.). Recording sites within the PMn were marked in four animals by means of extracellular deposits of Pontamine Sky Blue (PSB). PSB was iontophoresed (1–5 $\mu$A, negative DC) from a recording micropipette filled with PSB 2% in NaAc 0.5 M (pH 8.3; resistances 10–14 MΩ; Lee et al., 1969).

For intracellular recordings, electrodes were filled with 3 M KCl (25–30 MΩ) and, in experiments in which intracellular labeling was conducted, the recording electrode was filled with a solution of Biocytin (2% in 0.5 M KCl, 30–50 MΩ). Biocytin was iontophoresed using 500 ms current pulses of 1–2 nA with alternate polarities at 1 Hz for 5 min to 1 h. Usually one cell was labeled per experiment. M-cell axons were stimulated at the spinal cord with rectangular current pulses (0.15–0.3 mA, 0.2–0.5 ms), which, except when otherwise indicated, were sufficient to activate both M- axons. This was determined by the amplitude of M-AIR (see Falconi et al., 1995) and confirmed during extracellular recordings from the left M-cell by the appearance of the characteristic sequence of electrical events produced by the activation of one or both M-cell axons at the spinal cord (see Borde et al., 1991). When testing for the frequency sensitivity of M-cell-stimulation-induced responses, the M-cell axons were repetitively activated at low rate (mean 0.12 Hz, range 0.1–0.15 Hz) or high rate (mean 9.3 Hz, range 8.3–9.5 Hz). Stimuli were delivered phase-locked with a delay of 5 ms following the EOD. Therefore, stimulation rates depended to some extent on EOD frequency and showed minor variations around the desired values. Because of variations in the fish length, the distance between the stimulating and recording electrodes (conduction distance) varied considerably between experiments (7–12 cm). In order to compare data from different animals, peak latencies of faster evoked potentials were normalized to a conduction distance of 100 mm (peak latency$_{100\ mm}$) according to the formula:

$$\text{peak latency}_{100\ mm} = \textit{peak latency}_x \times 100/x.$$

where *peak latency*$_x$ corresponds to the latency to the peak in ms of a given potential for a conduction distance of $x$ mm. The normalization procedure assumes that changes in peak latency for a given evoked potential are only due to changes in the conduction distance. The possible contribution of variations in basic properties (i.e. utilization time and conduction velocity) of neural elements responsible for a given evoked potential with fish length were neglected. Electrical signals were stored on magnetic tape and acquired on a Macintosh IICi microcomputer with specially designed software for the analysis of data. Usually 50–100 single traces were averaged. For averaged responses to spinal cord stimulation at a high rate, field potentials evoked by the first 20 to 50 stimuli were excluded; at this time, the electromotor response, as well as other M-cell-dependent responses (for example, the collateral inhibition) consistently vanished (Furshpan and Furukawa, 1963; Hackett and Faber, 1983). The EOD was monitored during the experiment with head positive-tail negative electrode arrangement. Superscope software (GW Instruments, Somerville, MA, USA) was utilized to construct instantaneous frequency versus time plots.

For histological analysis, animals were deeply anesthetized by immersion in iced water. Subsequently, brains were removed and fixed overnight by immersion in paraformaldehyde (4%), and then embedded in gelatin (5%), mounted in a Vibroslicer (Campden, Lafayette, IN, USA) and serially sliced (75 $\mu$m) in the transverse plane. Biocytin-labeled cells were visualized using the Vectastain ABC System (Vector Laboratories, Burlingame, CA, USA) based on standard procedures as described by Horikawa and Armstrong (1988). Sections were counterstained with Pyronin-Y Red. Tissue shrinkage due to the foregoing histological procedures was assessed by injecting PSB at two different locations separated by a known distance (300 $\mu$m) along a vertical electrode track (see Fig. 2A). Shrinkage of approximately 25% was estimated and all measured parameters were corrected accordingly.

The same micropipette was used for glutamate antagonist application and field potential recording at the PMn (Fig. 1) following the experimental procedures described by Curti el al. (1999). Drugs were pressure ejected (Picospritzer II, General Valve Corporation, Fairfield, NJ, USA) by pulses of 20–50 p.s.i. and 10–500 ms duration. In air, ejected solution droplets were 10–30 $\mu$m in diameter. Based upon the formula: $4/3\ \pi r^3$, where r is the radius of the droplet, the volumes that were ejected ranged from 0.5–15 pl. The micropipette filling solutions (dissolved in 154 mM NaCl) were ($\alpha$)-2-amino-5-phosphonopentanoic acid (AP5, 500 $\mu$M) and 6-cyano-7-nitroquinoxaline-2,3-dione HBC-complex (CNQX, 1–3.9 mM). These substances were purchased

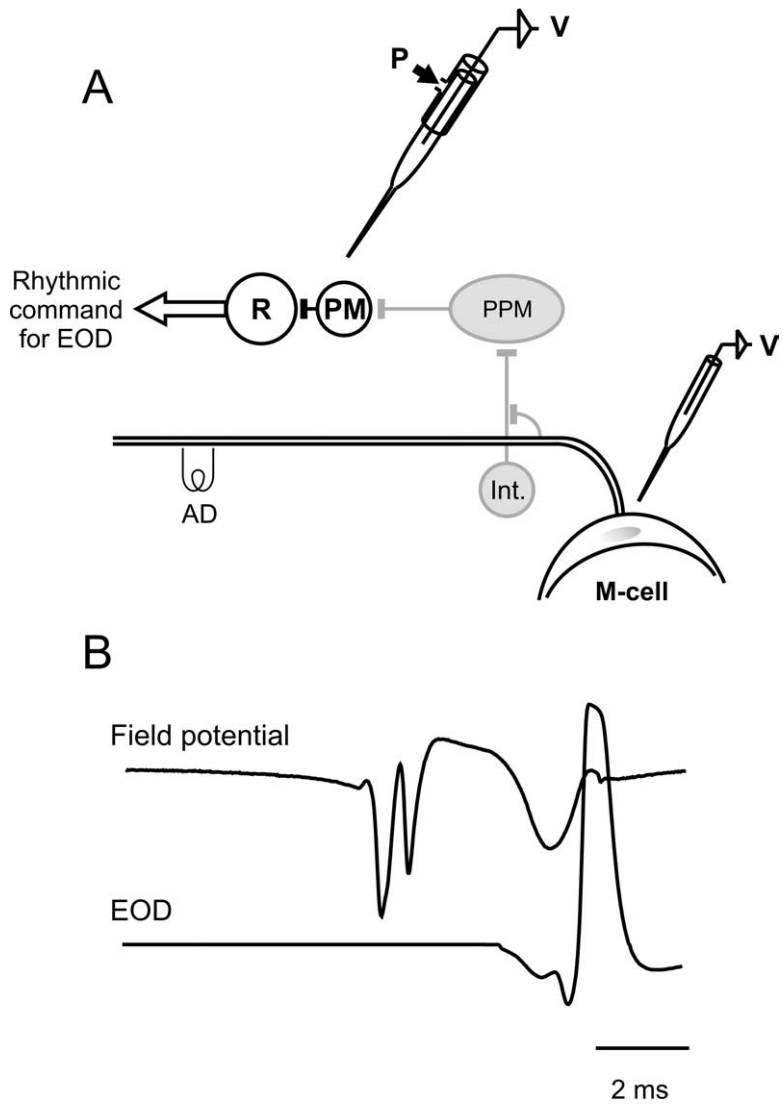


**Fig. 1.** (A) Diagram showing the putative neural circuit that mediates the M-cell-initiated electromotor behavior and the experimental paradigm. The arrangement of micropipettes for extracellular recording (V) and pressure injection (P), as well as electrodes for antidromic activation of the M-cell (AD) is depicted. The M-cell probably innervates an as-yet-unidentified group of interneurons (Int.), which in turn innervates several prepacemaker structures (PPM). The cellular types that compose the PMn are also depicted, PM and relay cells (R). Extracellular recordings were obtained at different levels within the PMn, and in some experiments an additional recording electrode was placed near the M-cell soma. During pharmacological experiments the same electrode was used for both glutamate antagonist pressure injections and field potential recordings near PM cells. (B) Phase-locking between PMn activity and EOD. The traces depict simultaneous recordings of the spontaneous PMn field potential (upper trace) and the EOD (lower trace) in a partially curarized animal. At this particular recording position, the field potential exhibited two sharp negative components (see text for further explanation). The traces are averages of approximately 100 consecutive single sweeps.

from RBI (Natick, MA). Student's *t*-test was used to assess the statistical significance of the data.

## RESULTS

Structural information of activated neural structures greatly facilitates the interpretation of extracellular field potentials produced by both spontaneous and evoked electrical activity (Llinás and Nicholson, 1974). Thus, a series of experiments using a combination of anatomical and electrophysiological techniques was first performed to obtain a detailed correlation between the spatial arrangement of neural elements that comprise the PMn in *Gymnotus carapo* and the particular waveform of field potentials produced by the spontaneous activity of the nucleus.

Spontaneous activity of the PMn was recognized as a compound field potential phase-locked with and preceding each EOD by about 3.5 ms (Fig. 1B). At 0 $\mu$m, field potentials exhibited two sharp negative components separated by a mean interval of 0.89 ms ($\pm$0.19, $n$=11). As indicated by the extracellular marking with PSB, the maximal amplitude of the first negative component (0 $\mu$m) was recorded in the proximity of PM-cell somas, whereas the maximal amplitude of the second negative component was recorded more ventrally near the somas of the relay cells

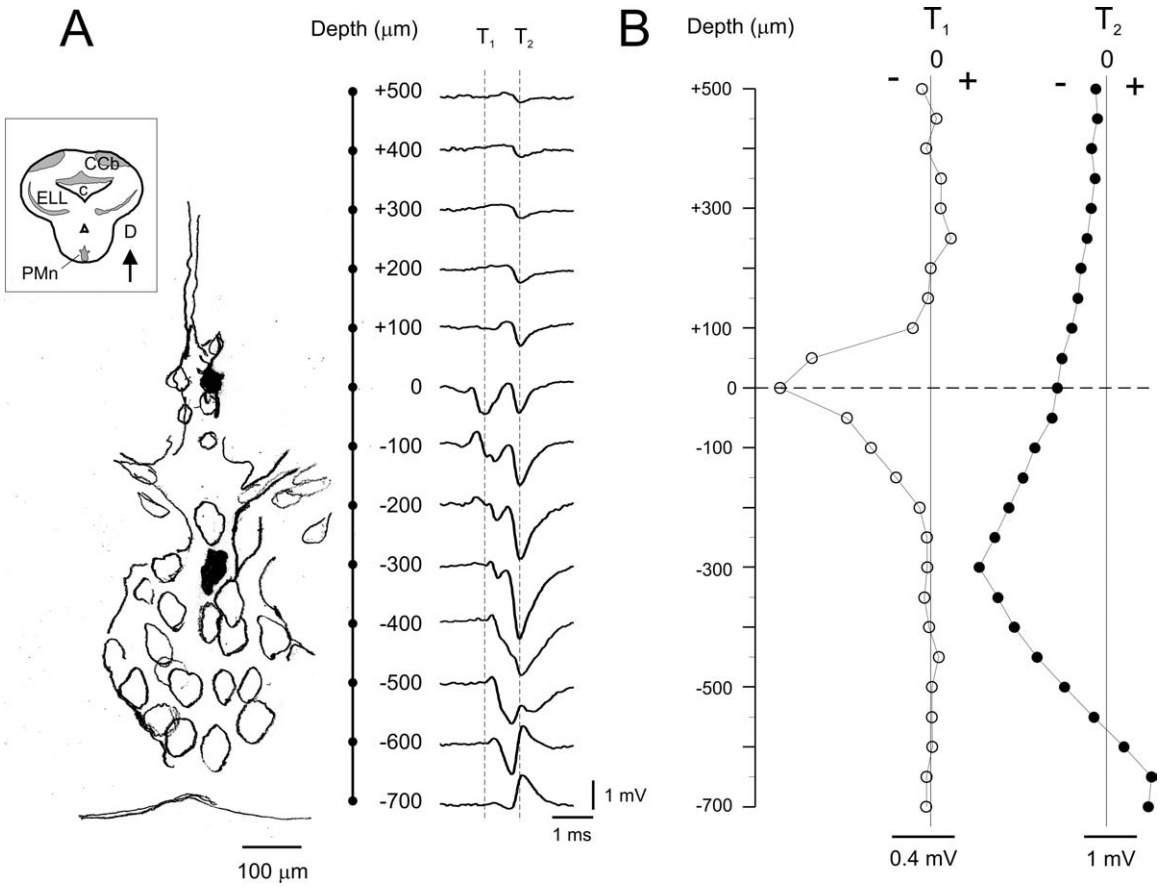


**Fig. 2.** Spatial variation of PMn spontaneous field potentials along the dorso-ventral axis. (A) Left. Camera lucida drawing of a transversal section of the PMn. The somas of PM cells are dorsal whereas the somas of the relay cells are located in the ventral portion of the nucleus. The ventral surface of the medulla is also illustrated. The black spots represent two PSB deposits separated by 300 $\mu$m, one is observed near PM cell somas and the other near relay cell somas. Inset: schematic drawing of a transversal section of the fish brain at the PMn level including the main anatomical landmarks: c, cerebello-medullary cistern; CCb, corpus cerebelli; ELL, electrosensory lateral line lobe. The arrow indicates dorsal direction (D). Right. Depth series of spontaneous PMn field potentials recorded along a dorso-ventral electrode track passing near the midline. Black dots along the vertical line at left represent the successive recording positions. Recordings were made at known distances (indicated by the numbers at left) from the level at which the first negative potential attains its maximal amplitude (labeled 0 $\mu$m, dorsal PSB deposit at left). Positive values indicate positions dorsal to this level whereas negative values correspond to ventral positions. At $-300$ $\mu$m (ventral PSB deposit in the drawing) the second negative potential was maximal. Each record represents the average of 100 single traces. Vertical dotted lines (T1 and T2) indicate the times at which the first and second negative components attain their maximal amplitudes respectively. Field potentials were aligned, taken as reference the occurrence of the EOD (not shown). (B) Depth profiles of the first and second components of PMn spontaneous field potentials illustrated in A. Plots of field potential amplitude (abscissa), at the times indicated in A right (T1 and T2), as a function of depth (ordinates, at the same scale used in A). In this example, field potentials were measured at a depth step of 50 $\mu$m. The horizontal dashed line indicates the level 0 $\mu$m.

(Fig. 2A). The spatial distribution of these two components is better illustrated in the depth profile shown in Fig. 2B. The first negative component (T1 in Fig. 2B) reached maximum amplitude near PM cell somas, and coincided with a small positive potential at dorsal positions (from $+200$ to $+400$ $\mu$m labels in Fig. 2B). Conversely, the second negative component (T2 in Fig. 2B) attained its maximum amplitude at the level of relay cell somas ($-300$ $\mu$m). This potential was associated with a positive potential observed at even more ventral recording sites ($-600$ to $-700$ $\mu$m). Since PM cell somas are located in a dorsal position while relay cell somas are located ventrally within the nucleus, the first negative component most likely corresponds to the synchronized discharge of PM cells, whereas the second negative component most probably results from synchronized activation of relay cells. This interpretation was further evaluated by determining, in the same animal, the timing of the two negative components of extracellular field potentials and the intracellular activity of electrophysiologically and morphologically identified cells (Fig. 3). The morphological characteristics of identified neurons obtained in these experiments provided critical structural details that helped for the analysis of both spontaneous and evoked field potentials. PM cells were identified based on their spontaneous rhythmic discharge phase locked with the EOD and the presence of a typical pacemaker potential preceding each spike (Fig. 3A left, Bennett et al., 1967; Falconi et al., 1997). The soma mean diameter of PM cells was 27.1 $\mu$m ($\pm$10.5 STD, $n=5$); these cells were located in the dorsal aspects of the nucleus together with their main dendritic branches (Fig. 3A right). Thin apical den-

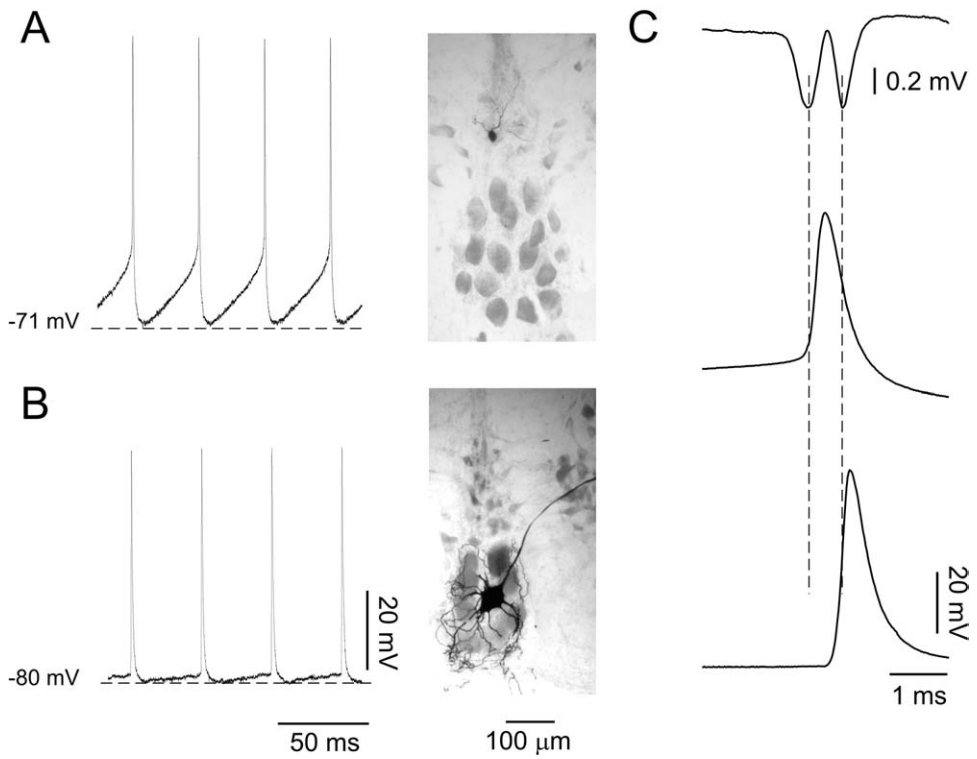


**Fig. 3.** Identification of neuronal elements responsible for PMn spontaneous field potentials. (A) Electrophysiological and morphological characterization of PM cells. Left, intracellular recording from a representative PM cell showing the main electrophysiological features of this cellular type, i.e. spontaneous rhythmic discharges preceded by the pacemaker potential (the depolarizing slope between spikes). Right, transversal section of the PMn showing the Biocytin-filled PM cell recorded at left. (B) Electrophysiological and morphological characterization of relay cells. Left, intracellular recording from a representative relay cell. Typically, this cellular type exhibits spontaneous rhythmic discharge as PM cells, but the pacemaker potential is absent. Right, merge of two successive PMn transversal sections showing the biocytin-filled relay cell recorded at left. In A and B, left panels, the membrane potential indicated by the dashed line is included as reference (values at left). Transversal sections shown in A and B, right panels, were counterstained with Pyronine-Y Red. (C) Temporal correlation between PMn spontaneous field potential recorded at 0 $\mu$m (upper trace) and intracellular activity of PM and relay cells (middle and lower traces respectively). These recordings were successively obtained in the same animal and were aligned taking the EOD as a temporal reference. As indicated by the vertical dashed lines, the peak of the first and second negative components of the field potential recording occurred during the rising phase of the PM cell and relay cell action potentials respectively. Each recording in this figure represents averages of 100 single traces.

dritic branches were observed traveling vertically within the medullary raphe (data not shown).

At ventral locations, impaled relay cells also exhibited spontaneous rhythmic discharges that were phase-locked with the EOD; however, their action potentials arose abruptly from the base line (Fig. 3B, left). These cells showed a large cell body with a mean diameter of 64.5 $\mu$m ($\pm$26.1 STD, $n$=4), an extensive dendritic field surrounding adjacent relay cell-somas and a large diameter axon leaving the nucleus in a dorsolateral direction (Fig. 3B, right). A representative example of the temporal correlation between the discharge of PM and relay cells recorded intracellularly and the two negative components of the field potential recorded at 0 $\mu$m is illustrated in Fig. 3C. In this example, the peak of the first negative component preceded the peak of the PM cell action potential by 0.3 ms and the peak the second negative component occurred 0.15 ms before that of the relay cell discharge. Although the exact timing between extra and intracellular events for a given cellular type showed minor variations, in all cases the peak of the negative potential occurred during the rising phase of the action potential recorded intracellularly. The mean interval between the peaks of both electrical events was 0.57 ms ($\pm$0.059 STD, $n$=4) and 0.37 ms ($\pm$0.15 STD, $n$=8) for PM and relay cells respectively.

The preceding results shed light on the relationship between spontaneous electrical events and morphological details of the PMn in *Gymnotus carapo*. Synchronized activation of PM cells sets up the first negative component of the spontaneous PMn field potential, which is maximal (at 0 $\mu$m) near the center of a region of the PMn containing the somas of PM cells together with their main perisomatic dendritic branches. In turn, the second negative component results from the synchronized discharge of relay cells and attains its maximal amplitude at a recording site (at $-$300 $\mu$m) characterized by the presence of relay cells' somas densely surrounded by their dendritic arborizations.

### PMn field potentials evoked by spinal cord stimulation

It has been demonstrated in *Gymnotus carapo* that M-cell activation is sufficient to provoke M-AIR (Falconi et al., 1995). In addition, results from electrophysiological and

pharmacological studies have indicated that M-AIR is produced by excitatory synaptic inputs to PMn (Falconi et al., 1997; Curti et al., 1999). We further studied these synaptic actions using extracellular recordings at different positions within the nucleus guided by the spontaneous field potential waveform (see above). As illustrated in Fig. 4A, low rate (mean 0.1 Hz) spinal cord stimulation that elicited M-AIR (left), also evoked in the vicinity of PM cells, a sequence of field potentials (right) that consisted of a short latency, brief negative–positive component, followed by a slow and long-lasting negative potential. Superimposed to this slow negative evoked potential, extracellular recordings exhibited repetitive negative sharp peaks due to spontaneous rhythmic activation of the PMn. Although in our experiments responses to 50–100 successive stimuli were averaged, PMn spontaneous field potentials were still observed because spinal stimuli were delivered phase-locked with EOD and the electromotor response is highly stereotyped (Falconi et al., 1995).

In the example illustrated in Fig. 4A (right), the slow and long-lasting negative evoked potential peaked between the first and the second spontaneous PMn field potential, about 30 ms after the spinal stimulus, and lasted for up to 400 ms. Similar waveform characteristics were observed in all experiments, with a mean peak latency of 47.8 ms (±14.07 STD), a mean peak amplitude of 0.2 mV (±0.91 STD) and a mean duration of 468.0 ms (±122.3 STD; $n=12$).

As with other well-characterized M-cell outputs, the magnitude of M-AIR is sensitive to high frequency stimulation and the response is eliminated at rates greater than 5–6 Hz (Hackett and Faber, 1983; Borde et al., 1991; Falconi et al., 1995; 1997). Thus, a frequency-dependent reduction of the associated slow negative evoked potential should be expected. The effect of high rate (mean 9 Hz) spinal cord stimulation on both M-AIR and evoked potentials is illustrated in Fig. 4B. Concurrently with the suppression of the electromotor behavior (Fig. 4B, left and inset), the peak amplitude of the slow negative potential was reduced to 14% of that recorded during control conditions (Fig. 4B, right). Similar effects were observed in all experiments with a mean reduction of the peak amplitude to 12.2% (±8.0 STD; $n=11$) of low rate stimulation values.

Short latency negative components of potentials elicited by low and high stimulation rates are illustrated in Fig. 4C. Low rate stimulation (thick trace) evoked two successive negative potentials that peaked at 1.2 ms (filled circle, Fig. 4C) and at 2.4 ms (asterisk, Fig. 4C) after the stimulus artifact. In the 14 animals tested, the first negative potential showed a mean peak latency$_{100\ mm}$ of 2.0 ms (±0.41 STD), a mean peak amplitude of 0.36 mV (±0.25 STD) and was followed by the second negative peak after a mean interval of 0.91 ms (±0.29 STD) which exhibited a mean peak amplitude of 0.73 mV (±0.22 STD). These negative components differed in their sensitivity to high frequency stimulation. Whereas the first negative peak remained unchanged following high rate stimulation, the identical stimulation paradigm produced a substantial reduction of the second negative peak (Fig. 4C, thin trace; mean reduction to a 15.2%, ±7.64 STD of low rate stimulation amplitudes). The depth profile of the first negative peak showed maximum amplitude at −100 $\mu$m and inverted its polarity between −200 $\mu$m and −300 $\mu$m, at the level where relay cell somas were located (Fig. 4D). According to its short latency, resistance to high frequency stimulation and spatial distribution, the first negative evoked potential most likely resulted from antidromic activation of relay cells whose axons distributed more caudally at the spinal cord (Ellis and Szabo, 1980).

We then focused on the PMn evoked field potentials associated with M-AIR that, as the electromotor behavior, vanished during high frequency stimulation. These M-AIR-related potentials consisted of an early peak (asterisk in Fig. 4C) and the slow and long-lasting negative potential (Fig. 4A, right). The former component will be herein referred as ENEP (for early negative evoked potential) and the latter as LNEP (for late negative evoked potential). A positive phase was usually observed during low rate spinal cord stimulation immediately following the ENEP (see for example Fig. 4A and C). The fact that the amplitude and duration, as well as the peak latency of the positive-going phase varied remarkably among experiments precluded any systematic quantitative study and was not further analyzed.

The correlation between these negative evoked potentials and M-AIR suggests that ENEP and LNEP are both initiated by M-cell activation. In order to test this possibility, in four animals extracellular electrical activity evoked by spinal cord stimulation was simultaneously recorded from the M-cell soma and the PMn while the EOD was monitored. A representative example of the results from this experimental series is illustrated in Fig. 5. Low rate spinal cord stimulation at intensities subthreshold for M-cell axons (Low rate/Sub., Fig. 5A) did not evoke any of the M-AIR-related PMn field potentials, i.e.: ENEP and LNEP (PMn, Fig. 5A). Only the short latency negative potential presumably due to antidromic relay cells activation was observed (filled circle in Fig. 5A, inset). As already demonstrated by Falconi et al. (1995), spinal stimuli at intensities just below threshold for M-cell axons did not produce any noticeable change in EOD frequency (Fig. 5A, EOD).

When threshold was reached for both M-cell axons during low rate stimulation (Low rate/Supra., Fig. 5B), an antidromic extracellular spike followed by a compound positive potential, the so-called extrinsic hyperpolarizing potential (EHP, oblique arrow) was recorded near the M-cell soma (Fig. 5B, M-cell). The EHP results from the activation of inhibitory interneurons that belong to the recurrent inhibitory circuit of M-cells (Faber and Korn, 1978; Borde et al., 1991). Concomitant with M-cells recruitment, ENEP (asterisk, Fig. 5B inset) and LNEP (Fig. 5B, PMn) were observed at the PMn, and a typical M-AIR was elicited (Fig. 5B, EOD). As expected with this higher stimulus intensity, the presumed relay cells antidromic potential increased in amplitude (filled circle, Fig. 5B inset). Simultaneous recording from the M-cell soma and the PMn allowed evaluating the relative timing of evoked potentials at these two separated regions; the M-cell antidromic spike

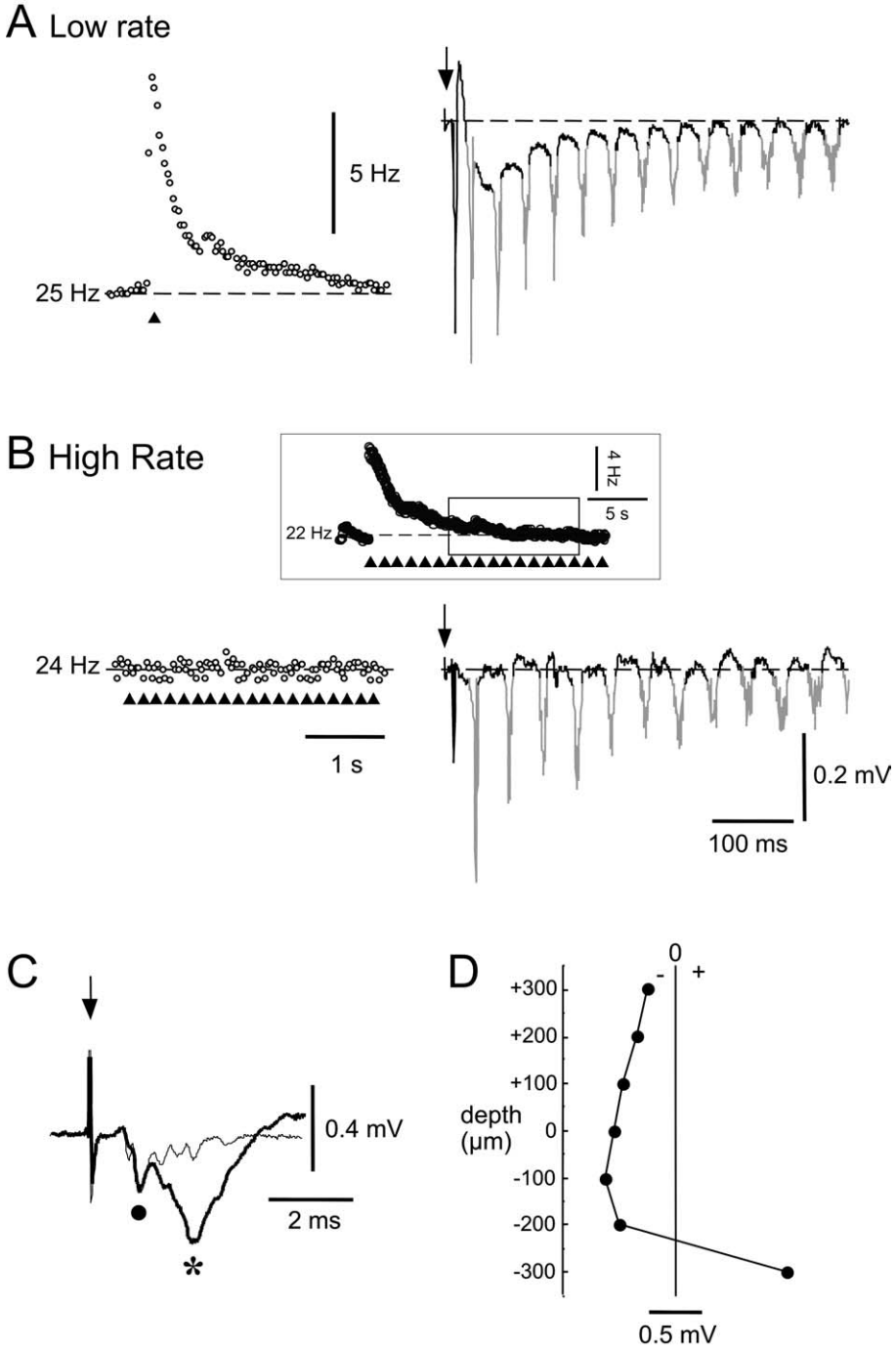


**Fig. 4.** M-AIR-related field potentials at the PMn. (A) Low rate spinal cord stimulation (mean 0.1 Hz). Left, plot of EOD frequency versus time showing the M-AIR elicited by M-cell axon activation at the time indicated by the arrowhead. M-AIR peak amplitude is 9 Hz and its duration is about 3.5 s. Right, averaged field potential recorded at 0 $\mu$m during M-AIR. The repetitive sharp negative peaks due to the spontaneous PMn activity were colored in gray for clarity. (B) High rate spinal cord stimulation (mean 9 Hz). Same structure as in A. Note the absence of the M-cell initiated electromotor behavior (left, arrowheads indicate only one stimulus every two or three). Along with the suppression of the M-AIR, high frequency stimulation also abolishes the slow and long lasting negative potential. Inset in B, EOD frequency versus time plot showing the first 20 s of the high-frequency stimulating protocol. The boxed area represents the responses that were included in the averages (approximately 100, after discarding the first 50 responses following the onset of the stimulation protocol; please see Experimental Procedures). Note that in this temporal window the M-AIR is almost suppressed. The dashed line in A and B left and in the inset, indicates the basal pre-stimulus frequency (values at left). In A and B right, the dashed line represents the 0 mV potential and the downward arrow indicates the stimulus artifact. (C) Superimposed and aligned first 7 ms of traces shown in A (thick trace) and B (thin trace). Note that high rate spinal cord stimulation abolishes the second negative component (asterisk) whereas the first one (filled circle) remains unaffected. The downward arrow indicates stimuli artifacts. (D) Depth profile of the first negative component indicated in C by the filled circle. Plot of field potential amplitude (abscissa) as a function of depth (ordinates) recorded at a depth step of 100 $\mu$m. Note the change in polarity of this wave between $-200$ and $-300$ $\mu$m, at the level of relay cell somas.

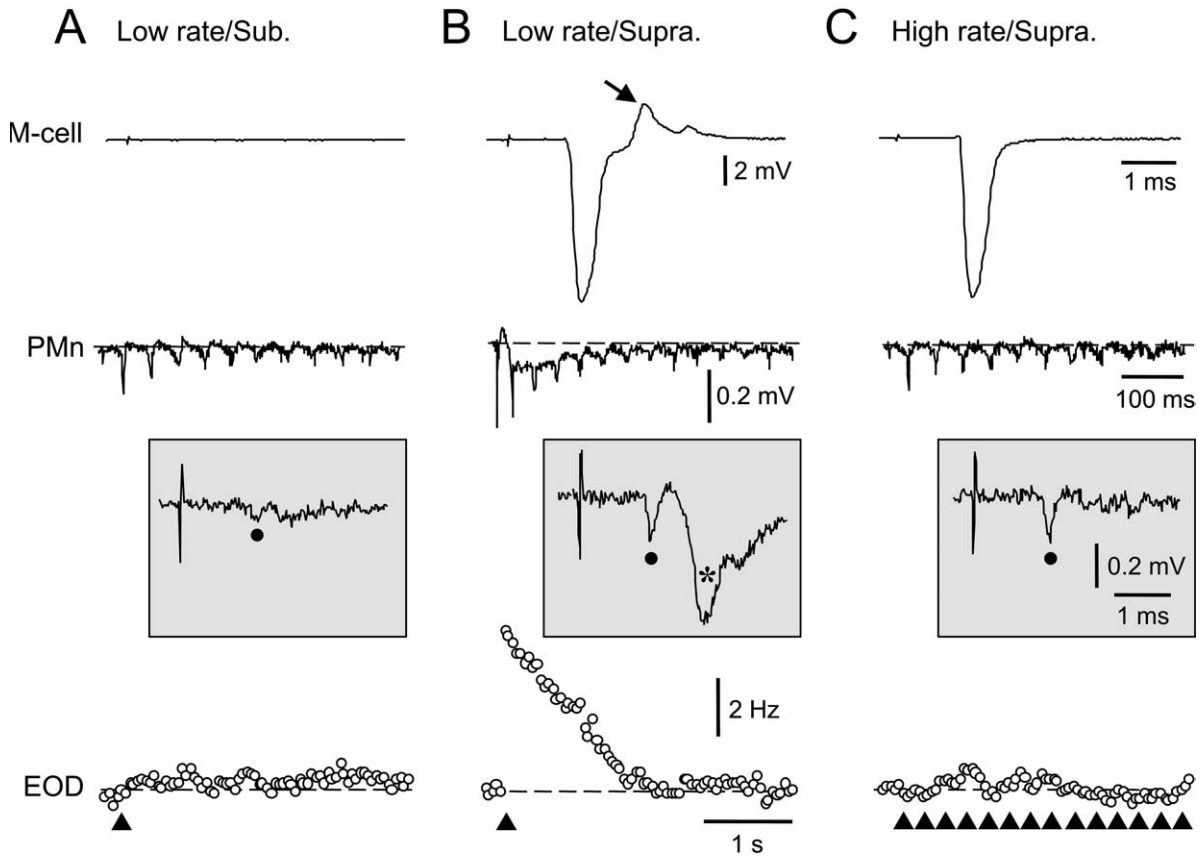


**Fig. 5.** Correlation between M-cell activity, evoked field potentials at the PMn and EOD rate modulations. Extracellular recordings were simultaneously obtained near M-cell axon cap (upper traces, M-cell) and within the PMn at 0 $\mu$m level (middle traces, PMn), while EOD rate was monitored (frequency versus time plots in lower panels, EOD) during stimulation with three different protocols (A, B and C). Insets: first 5 ms of the corresponding PMn evoked field potentials, depicted at an expanded temporal scale. (A) Low rate (mean 0.15 Hz) spinal cord stimulation subthreshold for M-cell axons (Low rate/Sub.). The absence of M-cell activity (upper trace) is correlated with the lack of M-AIR related potentials at the PMn (ENEP and LNEP), only a small negative potential is observed at a short latency (black dot, inset). As expected, this stimulating protocol did not evoke any significant change in EOD rate (lower trace). (B) Low rate (mean 0.15 Hz) spinal cord stimulation suprathreshold for both M-cell axons (Low rate/Supra.), as indicated in the upper trace by the presence of the characteristic all or none, short latency and large amplitude antidromic extracellular spike followed by the EHP (oblique arrow). Along with M-cell activation, LNEP (middle trace) and ENEP (asterisk, inset) were observed at PM cell somas level. As shown in the lower trace, low rate M-cell activation evoked a typical M-AIR. (C) High rate (mean 9.3 Hz) spinal cord stimulation suprathreshold for M-cell axons (High rate/Supra.). M-cell axons were still activated at the spinal cord level but the recurrent inhibitory circuit was no longer recruited, as suggested by the absence of the EHP (upper trace). Both M-AIR related negative potentials, LNEP and ENEP, were abolished whereas the shorter latency negative potential was still observed (filled circle, inset). High rate spinal cord stimulation also eliminated the electromotor behavior (lower trace). Dashed horizontal line in PMn field potential recordings represents the 0 mV potential. In EOD rate plots, arrowheads indicate the time of stimulation except in C where only one stimulus every two or three is illustrated. The basal pre-stimulus EOD frequency indicated by the dashed line was 17 Hz.

preceded the ENEP by a mean latency of 0.8 ms ($\pm$0.14 STD; $n$=4).

During high rate spinal cord stimulation at intensities suprathreshold for both M-cell axons (High rate/Supra., Fig. 5C), the antidromic M-cell spike was still evoked but the EHP was blocked indicating that the recurrent inhibitory circuit was no longer activated (Fig. 5C, M-cell). At the same time, both ENEP and LNEP vanished (Fig. 5C, PMn and inset), and the M-cell initiated electromotor behavior was abolished (Fig. 5C, EOD). In contrast, the presumed relay cells' antidromic potential was not affected by high rate spinal cord stimulation (filled circle, Fig. 5C inset).

Our data indicate that both ENEP and LNEP are closely related to M-AIR and all three are elicited by M-cell activation. This suggests that ENEP and/or LNEP might be produced by synaptic inputs to the PMn responsible for M-AIR. To further investigate the neural basis of these evoked potentials, we studied their spatial distribution within the PMn. Depth series of M-cell evoked potentials recorded from +300 $\mu$m to −300 $\mu$m with a depth step of 100 $\mu$m were obtained, and depth profiles of their peak amplitudes were then constructed. A representative depth series is illustrated in Fig. 6A at two different temporal scales. Normalized and averaged depth profiles of LNEP and ENEP peak amplitudes obtained in nine animals are depicted in Fig. 6B. The spatial distribution of these two M-AIR related potentials differed markedly. LNEP amplitude was maximal at PM cells somas level (0 $\mu$m), and progressively decreased to a 37.7% ($\pm$7.5 STD) and to a 50.9% ($\pm$14.2 STD) at +300 and −300 $\mu$m respectively (Fig. 6B, left). In contrast, ENEP amplitude gradually raised from ventral (−300 $\mu$m) to dorsal (+300 $\mu$m) re-

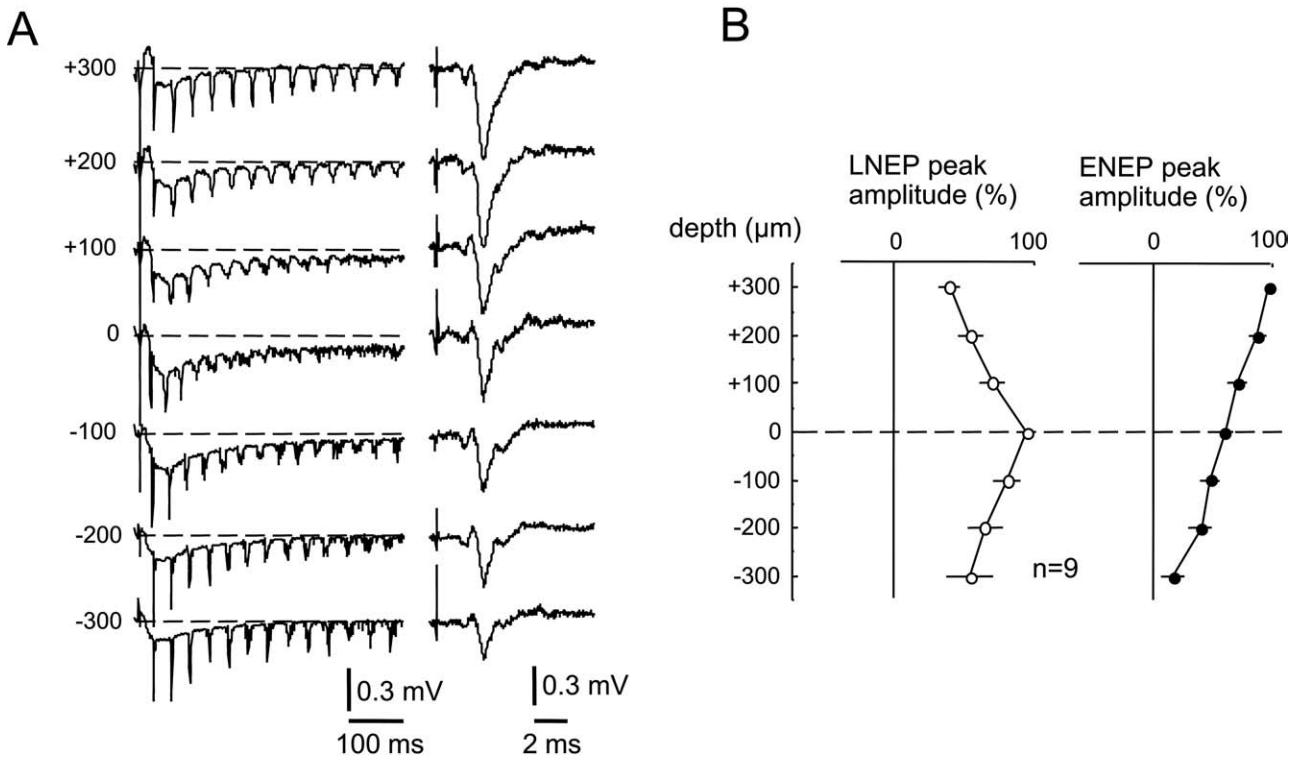


**Fig. 6.** Spatial variation of LNEP and ENEP within the PMn along the dorso-ventral axis. (A) Left, depth series of PMn field potentials evoked by low rate (mean 0.12 Hz) M-cell activation and recorded at a depth step of 100 $\mu$m (depth indicated by numbers at left). Right, initial 9 ms of the corresponding traces shown at left depicted at an expanded temporal scale. Horizontal dashed lines indicate the 0 mV potential. (B) Depth profile of LNEP (open circles, left) and ENEP (filled circles, right). Plots of field potential peak amplitudes normalized to their maximums (abscissa) as a function of depth (ordinates). Each point is the average of nine experiments, error bars represent STD.

cording positions (Fig. 6B, right). The amplitude of ENEP at $-300$ $\mu$m was a 26% ($\pm$9.1 STD) of its value at $+300$ $\mu$m. In some experiments, recordings were also obtained at even more distant locations from PM cell somas in the dorsal direction ($+400$ $\mu$m to $+600$ $\mu$m) and the amplitude of the ENEP further increased (data not shown).

The results presented in this section show that ENEP and LNEP are both dependent on M-cell activation. Moreover, whereas ENEP seems to be generated by neural elements located dorsal to and outside the PMn, LNEP is generated at the level of PM cells somas. This suggests that only LNEP is caused by excitatory synaptic inputs to PM cells responsible for M-AIR.

### Effects of AP5 and CNQX on M-AIR- and PMn-evoked potentials

Based on the effects of glutamate receptor blockers on M-AIR, Curti et al. (1999) concluded that this electromotor behavior depends on the activation of NMDA and metabotropic glutamate receptors in PM cells. Moreover, even though PM cells are also endowed with functional ionotropic non-NMDA glutamate receptors, these receptors do not participate in the M-AIR. Since the aforementioned concepts were inferred from studies on the electromotor behavior, we designed a series of experiments in order to obtain *direct* evidence for the role played by the different ionotropic glutamate receptors in PM cells vis-à-vis the M-AIR response. These experiments consisted of testing the effects of specific NMDA (AP5) and non-NMDA (CNQX) receptor blockers on LNEP. Recording electrodes filled with the blocker solution were positioned at 0 $\mu$m and both LNEP and M-AIR were evoked before, 2 min and 20 min after AP5 or CNQX injections. An example of AP5 effects on LNEP is illustrated in Fig. 7A. In this experiment, AP5 injection reduced the peak amplitude of LNEP to a 57% of control values (lower trace, AP5). Concomitantly with the suppressor effect of AP5 on LNEP, there was a reduction of the M-cell initiated electromotor behavior to a 46.3% of control (Fig. 7B). The amplitude of both LNEP and M-AIR partially recovered 20 min after the injection to 85% and 83% of controls respectively (not shown). In contrast, neither LNEP nor M-AIR was affected by CNQX injections, as illustrated in Fig. 7C and D. Similar results were observed in two animals (three injections) where LNEP and M-AIR amplitudes averaged 103.3% ($\pm$3.8 STD; $P>0.615$) and 99.1% ($\pm$5.5 STD; $P>0.874$) of their control values respectively.

AP5 effects on evoked potentials and the electromotor behavior are summarized in Fig. 7E (left). Average amplitudes of LNEP and M-AIR two minutes after antagonist injections were 49.6% ($\pm$15.0 STD; $P<0.006$) and 47.5% ($\pm$13.4 STD; $P<0.004$) of their control values respectively ($n=4$). Both LNEP and M-AIR partially recovered to 85% ($\pm$10.9 STD) and 76.4% ($\pm$13.4 STD) of their initial values

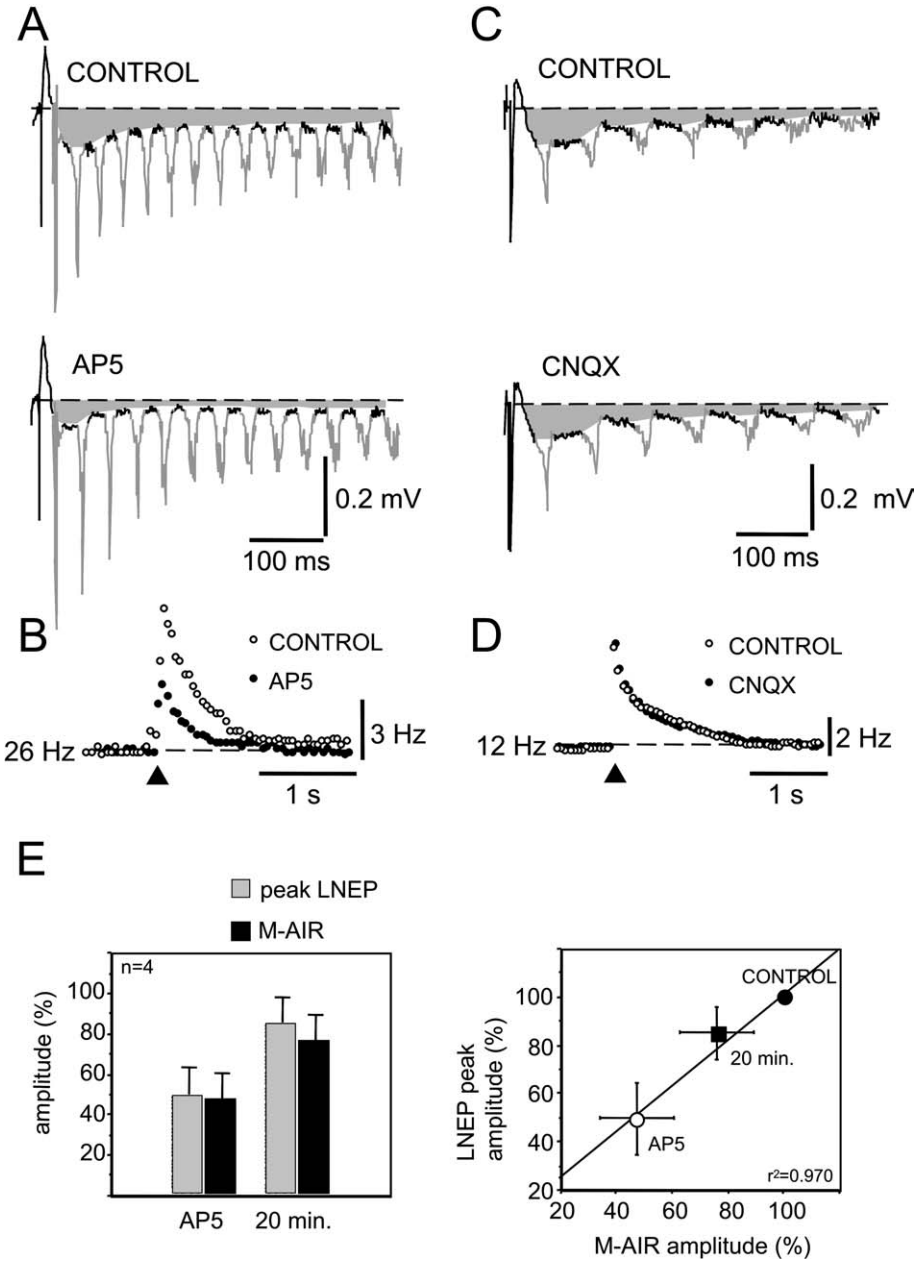


**Fig. 7.** Effects of ionotropic glutamate receptor antagonists (AP5 and CNQX) on LNEP and M-AIR. (A) Field potentials recorded at 0 $\mu$m during low rate (mean 0.11 Hz) spinal cord stimulation before (CONTROL) and 2 min after AP5 pressure injection (AP5; 500 $\mu$M, 50 ms, 20 p.s.i.). Recordings represent the average of 100 single traces. Spontaneous PMn field potentials were colored in gray for clarity. In the recordings illustrated in A and C the areas comprised between the pre-stimulus baseline potential (0 mV, dashed lines) and the estimated waveforms of LNEP were shaded to illustrate more clearly the effect of drug application. (B) Single M-AIRs (plots of EOD frequency versus time) before (CONTROL, open circles) and 2 min after AP5 application (AP5, filled circles) obtained during the stimulating protocols that evoked field potentials recordings depicted in A. Arrowhead indicates the time at which M-axons were stimulated at the spinal cord level. Dashed line indicates basal pre-stimulus frequency (value at left). (C) Same as A in a different fish in which CNQX was pressure injected (1.2 mM, 35 ms, 30 p.s.i.) near PM cell somas. (D) Single M-AIRs (plots of EOD frequency versus time) before (CONTROL, open circles) and 2 min after CNQX application (CNQX, filled circles) obtained during the stimulating protocols that evoked field potentials recordings depicted in C. (E) Left, amplitudes (mean±STD, $n$=4) of LNEP and M-AIR, obtained 2 min (AP5) and 20 min (20 min) after AP5 application are plotted as percentage of their control amplitudes. Right, plot of LNEP peak amplitude (ordinates) versus M-AIR amplitude (abscissa) expressed as percentage of their control values (mean±STD, $n$=4), obtained before (CONTROL, filled circle), 2 min after (AP5, open circle) and 20 min after (20 min, filled square) AP5 application. The data were fitted with a straight line ($r^2$=0.970).

respectively at 20 min after the injections. Changes in the electromotor behavior amplitude were paralleled by similar changes in the peak amplitude of LNEP. This is illustrated in Fig. 7E (right), in which averaged and normalized LNEP peak amplitude was plotted against averaged and normalized M-AIR amplitude before (CONTROL), 2 min (AP5) and 20 min after AP5 injections. As shown data acceptably fitted to a straight line ($r^2$=0.97).

During the experiments described above, ENEP was not affected by either AP5 or CNQX injections (data not shown).

## DISCUSSION

The combination of intracellular recordings and field potential analysis of spontaneous and M-cell evoked activity in the PMn has enabled us to determine the synaptic inputs that are responsible for the EOD frequency modulation that occurs during M-AIR and to identify their postsynaptic target within the PMn. In addition, field potential analysis combined with local application of ionotropic glutamatergic antagonists at specific locations within the PMn allowed us to demonstrate that NMDA glutamate receptors are responsible for mediating EOD frequency modulation. It is important to note that the use of the waveform of spontaneous field potential as an electrophysiological indicator of the location of the recording electrode relative to the soma and neurites of both pacemaker and relay cells was paramount in the process of interpretation of our results.

The accuracy of field potential interpretation depends crucially on morphological knowledge of generating neuronal elements and their spatial arrangement (Hubbard et al., 1969; Llinás and Nicholson, 1974). Unfortunately, except for the brief report of Trujillo-Cenóz et al. (1993), cytoarchitectural description of the PMn of *Gymnotus carapo* has not been specifically addressed in the many available studies of the electromotor system of other gymnotiform species that include morphological data (Bennett et al., 1967; Kawasaki and Heiligenberg, 1989), some of which revealed important interspecies differences (see for an example Ellis and Szabo, 1980). In the present paper, Pyronin-Y Red staining of medullary transverse sections containing the PMn together with intracellular labeling of electrophysiologically identified pacemaker and relay cells provided valuable anatomical details for a more precise interpretation of field potentials produced by both spontaneous and evoked activity. Moreover, data obtained from specific recording sites that were marked with PSB yielded a detailed correlation between the spatial arrangement of neural elements that comprise the PMn in *Gymnotus carapo* and the particular waveform of field potentials produced by the spontaneous activity of the nucleus.

Anatomical information combined with electrophysiological data, allowed us to set forth the following sequence of events occurring at the PMn of *Gymnotus carapo* during the pacemaker cycle. As in other gymnotiform fish (see for review Heiligenberg, 1991 and Lorenzo et al., 2001) the pacemaker cycle is initiated by the synchronous activation of PM cells. The discharge of an action potential at these cells sets up the early negative component of the spontaneous field potential. This component attains its maximal amplitude at PM cell somas level, and its peak is temporally correlated with the rising phase of the action potential of these cells. Concurrent with the peak of the early negative component, a positive going potential occurs at dorsal recording sites (from $+250$ $\mu$m to $+350$ $\mu$m). As illustrated in Fig. 8A, the negative potential is most probably due to a net current sink occurring during PM cell somas discharge and the coincident positive potential most likely results from an associated source of currents in the PM cells apical dendrites (present paper and Trujillo-Cenóz et al., 1993). The neural command originated at PM cells is conveyed to relay cells with a delay of approximately 0.9 ms, whose activation subsequently gives rise to the late negative component. In turn, this component reaches its maximal amplitude at the level of the somas of relay cells ($-300$ $\mu$m), and is temporally correlated with the rising phase of these cells' action potential. Spatial distribution of field potentials produced by relay cells' activation may result from the distribution of extracellular currents illustrated in Fig. 8B. Synchronous activation of relay cells gives rise to a net current sink localized in the nuclear region where the somas of these cells are concentrated. The associated current source is apparently restricted to region situated near the ventral border of the nucleus, which is almost devoid of somas but most probably composed of relay cells' dendrites.

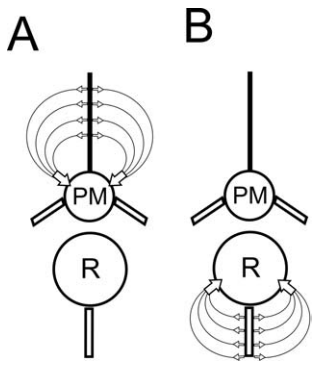


**Fig. 8.** Schematic of the possible distribution of extracellular currents at the PMn during pacemaker (T1, A) and relay cells (T2, B) activation. (A) At T1, the synchronous activation of PM cells gives rise to a net sink of currents at their somas and a current source at their apical dendrites. (B) At T2, synchronous activation of relay cells causes a net current sink at a location of the nucleus dominated by the presence of relay cells somas and a current source near the ventral surface of the medulla where the nucleus is apparently composed solely by their dendritic arborizations. In A and B, because of the highly synchronic activation of each cellular type and their spatial segregation within the nucleus, a single "ideal" pacemaker and relay cell is illustrated representing the average behavior of each cellular subpopulation.

### Origin of PMn field potentials evoked by spinal cord stimulation

Low rate spinal cord stimulation at intensities suprathreshold for M-cell axons evoked along with the M-AIR a series of negative field potentials at PMn. These field potentials were first characterized based on their sensitivity to high frequency stimulation. Whereas the shorter latency negative peak remained unaffected by high rate stimulation, the delayed potentials (ENEP and LNEP) were suppressed. Based on its resistance to high frequency stimulation, spatial distribution and graded amplitude with stimulus strength, we conclude that the shorter latency negative potential likely results from the antidromic activation of some relay cells. On the other hand, ENEP and LNEP

sensitivity to high frequency stimulation, together with the close correlation between these components, M-AIR, and M-cell antidromic spikes, strongly suggests that ENEP and LNEP depend on M-cell activation.

ENEP and LNEP show the same frequency sensitivity as M-AIR and EHP, two different well-demonstrated functional outputs of the M-cell system (Furshpan and Furukawa, 1963; Faber and Korn, 1978; Borde et al., 1991; Falconi et al., 1995, 1997). Indeed, simultaneous recordings showed that the drop-off of evoked potentials at high frequency stimulation was strictly correlated with a drop-off of the EHP on the M-cell. In most teleosts, M-cell-associated brainstem networks (motoneurons and recurrent inhibitory interneurons) are activated through specialized interneurons (cranial relay neurons, CRN) that are postsynaptic to M-cell axons (Hackett and Faber, 1983). The physiological properties of this M-cell output connection have been extensively studied (Hackett and Faber, 1983; Hackett et al., 1989). Characteristically, M-cell activation at 3–10 Hz produces a marked synaptic depression at this contact and consequently transmission to brainstem networks via the CRNs is blocked (Faber and Korn, 1978; Hackett et al., 1989; Borde et al., 1991; Waldeck et al., 2000). The sensitivity to high frequency stimulation of ENEP and LNEP strongly suggests that neural elements generating both evoked potentials are activated by M-cells through an output connection sharing the physiological properties of the M-cell–CRN synaptic contact.

The cellular origin of ENEP and LNEP seems to be different as suggested by their dissimilar spatial distribution. ENEP amplitude was greater at dorsal positions (+300 $\mu$m) than at 0 $\mu$m, indicating that this component results from the activation of structures located dorsally and outside the PMn. The delay between the M-cell spike and the ENEP (about 0.8 ms) is comparable to that reported in goldfish between M-cell spike and the postsynaptic action potential at cranial relay interneurons (Hackett and Faber, 1983; Waldeck et al., 2000). The axons of these interneurons run in the medial longitudinal fasciculus, a bilateral bundle of fibers located just beneath the ventricular surface (Hlavacek et al., 1984; Barry and Bennett, 1990). Thus, ENEP may result from the activation of similar cranial relay interneurons in *Gymnotus carapo* (Int. in Fig. 1) that mediate cranial components of the M-cell-initiated behavioral repertoire including the M-AIR.

On the other hand, LNEP amplitude reached a maximum at PM cells somas level (Fig. 6B). Previous work suggested that synaptic inputs responsible for M-AIR are restricted to PM cells' somas and/or basal dendrites (Falconi et al., 1997; Curti et al., 1999). Additionally, LNEP exhibited a time course resembling that of the postsynaptic potential recorded from PM cells during the M-AIR (see Fig. 5 from Falconi et al., 1997). Based on this evidence, we conclude that LNEP most likely results from the extracellular currents caused by M-cell-dependent excitatory synaptic actions on PM cells, an excitatory effect that is responsible for the M-AIR behavioral response.

### Ionotropic glutamate receptor subtypes involved in M-cell initiated synaptic actions on PM cells

Applying specific glutamate receptor antagonists near PM cells and studying their effects on M-AIR, Curti et al. (1999) concluded that this electromotor behavior is probably due to the activation of both NMDA and metabotropic receptors but not on non-NMDA receptors. Moreover, from the effects of specific glutamate agonists on EOD frequency, these authors obtained data indicating that non-NMDA ionotropic receptors are also expressed at PM cells. These results suggested that even though non-NMDA receptors are present at the postsynaptic cell they do not participate in M-AIR. That is, glutamate released from prepacemaker afferents activated during M-AIR acts on NMDA and metabotropic receptors but not on non-NMDA ionotropic receptors. This is striking since in most vertebrate glutamatergic synaptic contacts NMDA and non-NMDA ionotropic receptors are co-localized at the subsynaptic membrane and hence co-activated during normal transmission (Isaac, 2003).

In the present study, using the same micropipette for field potential recording and drug application at known positions within the PMn we were able to identify the M-cell-initiated excitatory potential, i.e. LNEP, and to test the effects of glutamate antagonists on this synaptic response. Injections of AP5 at 0 $\mu$m reversibly reduced LNEP and the M-cell-initiated electromotor behavior to a similar extent. In contrast, applications of CNQX at the same level did not affect the LNEP or EOD rate modulation. These results demonstrate that glutamatergic M-cell-evoked excitatory synaptic actions on PM cells, involve the activation of NMDA receptors *but not* of non-NMDA receptors. These data lead us to propose that these ionotropic glutamate receptors subtypes are not co-localized at the subsynaptic membrane of PM cells.

In mammals, pure NMDA glutamatergic synaptic contacts have been associated with the occurrence of postsynaptically silent synapses (Isaac et al., 1995; Liao et al., 1995). In this type of synapse, glutamate released from presynaptic terminals is unable to produce any detectable electrophysiological response at postsynaptic cells when recorded near the resting membrane potential, because of the voltage-dependent blockade of NMDA receptors by extracellular $Mg^{2+}$ (Nowak et al., 1984). At glutamatergic synapses activated during M-AIR, however, pure NMDA synaptic contacts are functional most probably owing to the fact that PM cells are spontaneously active neurons whose repetitive discharge may result in transient but repetitive relief of $Mg^{2+}$ blockade. Additionally, certain NMDA receptor variants may conduct at or near resting membrane potential as described in lower vertebrates and mammals (Berman et al., 1997; Wolszon et al., 1997; Harvey-Girard and Dunn, 2003; Cull-Candy et al., 2001). Thus, for a NMDA component to be manifest at these synapses, a concomitant non-NMDA receptor-mediated depolarization is not necessary.

We have demonstrated that, even though PM cells contain both NMDA and non-NMDA ionotropic glutamate

receptors, M-cell-initiated synaptic actions do not involve non-NMDA receptor subtypes. The much slower kinetics of NMDA receptors compared with that of non-NMDA receptors fit the temporal characteristics of the synaptic responses that were observed in our experiments (total duration about 400 ms, see Fig. 4A right). In fact, synaptic currents mediated by NMDA receptors exhibit a slow rise time (time to peak around 20 ms) and an exponential decay with time constants that could be in the order of 300 ms depending on receptor subunit composition. On the other hand, non-NMDA receptor-mediated synaptic currents typically rise in less than 1 ms and decay with a time constant of between 0.2 and 8 ms (Edmonds et al., 1995; Cull-Candy et al., 2001).

### Neural basis of M-AIR

Segregation of behavior-specific synaptic inputs to PM or relay cells of the PMn appears to be a common neural design of gymnotiform fish, producing diverse electromotor outputs (Spiro, 1997; Juranek and Metzner, 1998; Curti et al., 1999). For example, excitatory inputs restricted to PM cells may induce EOD frequency rises while similar inputs to relay cells produce abrupt EOD frequency increases accompanied by distortions of the EOD waveform (chirps; see for review Lorenzo et al., 2001). The former electromotor output, observed during exploratory behaviors, has been considered as a mechanism to enhance the electrolocative ability of gymnotiforms while the latter, often displayed during courtship, appears to be relevant as a communicatory signal. Consequently, excitatory inputs to PM cells where the rhythmic activity originates may increase EOD rate without changes of its waveform, preserving the EOD as a signal for active electrolocation. M-AIR consists of an abrupt and prolonged increase of EOD rate without modification of its waveform (Falconi et al., 1995). As demonstrated in the present study, activation of PM cells via NMDA receptors by M-cell glutamatergic inputs seems to be an efficient neural strategy to produce a long-lasting enhancement of the electrolocative sampling of the fish during M-cell-initiated motor behaviors.

*Acknowledgments—This work was partially supported by BID-CONICYT grant no. 353, PEDECIBA and CSIC, Univ. de la República. The authors thank Dr. Francisco Morales for his support, Dr. Washington Buño and Dr. Curtis Bell for critical comments on an earlier version of the manuscript. We are also indebted to Dr. Jack Yamuy for his helpful suggestions and assistance in English editing.*

## REFERENCES

Barry MA, Bennett MVL (1990) Projections of giant fibers, a class of reticular interneurons, in the brain of the silver hatchetfish. Brain Behav Evol 36:391–400.

Bennett MVL (1971) Electric organs. In: Fish physiology (Hoar WS, Randall DJ, eds), pp 493–574. New York: Academic Press.

Bennett MVL, Pappas GD, Gimenez M, Nakajima Y (1967) Physiology and ultrastructure of electrotonic junctions. IV. Medullary electromotor nuclei in gymnotiform fish. J Neurophysiol 30:236–300.

Berman NJ, Plant J, Turner RW, Maler L (1997) Excitatory amino acid receptors at a feedback pathway in the electrosensory system: implications for the searchlight hypothesis. J Neurophysiol 78: 1869–1881.

Black-Cleworth P (1970) The role of the electric discharges in the non-reproductive social behavior of Gymnotus carapo (Gymnotidae, Pisces). Anim Behav Monogr 3:1–77.

Borde M, Pereda AE, Morales FR (1991) Electrophysiological characteristics of the Mauthner cell of the weakly electric fish Gymnotus carapo. Brain Res 567:145–148.

Caputi A, Aguilera P (1996) A field potential analysis of the electromotor system of Gymnotus carapo. J Comp Physiol A 179: 827–835.

Cull-Candy S, Brickley S, Farrant M (2001) NMDA receptor subunits: diversity, development and disease. Curr Opin Neurobiol 11: 327–335.

Curti S, Falconi A, Morales FR, Borde M (1999) Mauthner cell-initiated electromotor behavior is mediated via NMDA and metabotropic glutamatergic receptors on medullary pacemaker neurons, in a gymnotid fish. J Neurosci 19:9133–9140.

Dye JC, Heiligenberg W, Keller CH, Kawasaki M (1989) Different classes of glutamate receptors mediate distinct behaviors in a single brainstem nucleus. Proc Natl Acad Sci U S A 86: 8993–8997.

Dye JC, Meyer JH (1986) Central control of the electric organ discharge of a weakly electric fish. In: Electroreception (Bullock TH, Heiligenberg W, eds), pp 72–102. New York: Wiley.

Edmonds B, Gibb AJ, Colquhoun D (1995) Mechanisms of activation of glutamate receptors and the time course of excitatory synaptic currents. Annu Rev Physiol 57:495–519.

Ellis DB, Szabo T (1980) Identification of different cell types in the command (pacemaker) nucleus of several gymnotiform species by retrograde transport of horseradish peroxidase. Neuroscience 5:1917–1924.

Faber DS, Korn H (1978) Electrophysiology of Mauthner cell: basic properties, synaptic mechanisms, and associated networks. In: Neurobiology of the Mauthner cell (Faber DS, Korn H, eds), pp 47–131. New York: Raven Press.

Falconi A, Borde M, Hernández-Cruz A, Morales FR (1995) Mauthner Cell-initiated abrupt increase of the electric organ discharge in the weakly electric fish Gymnotus carapo. J Comp Physiol A 176: 679–689.

Falconi A, Lorenzo D, Curti S, Morales FR, Borde M (1997) Mauthner cell-evoked synaptic actions on pacemaker medullary neurons of a weakly electric fish. J Comp Physiol A 181:143–151.

Furshpan EJ, Furukawa T (1963) Two inhibitory mechanisms in the Mauthner neurons of goldfish. J Neurophysiol 26:140–176.

Hackett JT, Faber DS (1983) Mauthner axon networks mediating supraspinal components of the startle response in the goldfish. Neuroscience 8:317–331.

Hackett JT, Cochran SL, Greenfield LJ Jr (1989) Quantal transmission at Mauthner axon target synapses in the goldfish brainstem. Neuroscience 32:49–64.

Hagedorn M (1986) The ecology, courtship, and mating of Gymnotiform electric fish. In: Electroreception (Bullock TH, Heiligenberg W, eds), pp 497–525. New York: Wiley.

Harvey-Girard E, Dunn RJ (2003) Excitatory amino acid receptors of the electrosensory system: the NR1/NR2B N-methyl-D-aspartate receptor. J Neurophysiol 89:822–832.

Heiligenberg W (1991) Neural nets in electric fish. Computational neuroscience series. Cambridge, MA: MIT Press.

Hlavacek M, Tahar M, Libouban S, Szabo T (1984) The mormyrid brainstem. I. Distribution of brainstem neurones projecting to the spinal cord in Gnathonemus petersii. An HRP study. J Hirnforsch 25:603–615.

Horikawa K, Armstrong WE (1988) A versatile means of intracellular labeling: injection of biocytin and its detection with avidin conjugates. J Neurosci Methods 25:1–11.

Hubbard JI, Llinás R, Quastel DMJ (1969) Extracellular field potentials analysis in the central nervous system. In: Electrophysiological

analysis of synaptic transmission, pp 265–293. Baltimore: Williams & Wilkins.

Isaac JT, Nicoll RA, Malenka RC (1995) Evidence for silent synapses: implications for the expression of LTP. Neuron 15:427–434.

Isaac JT (2003) Postsynaptic silent synapses: evidence and mechanisms. Neuropharmacology 45:450–460.

Juranek J, Metzner W (1998) Segregation of behavior-specific synaptic inputs to a vertebrate neuronal oscillator. J Neurosci 18: 9010–9019.

Kawasaki M, Heiligenberg W (1989) Distinct mechanisms of modulation in a neuronal oscillator generate different social signals in the electric fish *Hypopomus*. J Comp Physiol A 165:731–741.

Kawasaki M, Heiligenberg W (1990) Different classes of glutamate receptors and GABA mediate distinct modulations of a neuronal oscillator, the medullary pacemaker of a gymnotiform electric fish. J Neurosci 10:3896–3904.

Kawasaki M, Maler L, Rose GJ, Heiligenberg W (1988) Anatomical and functional organization of the prepacemaker nucleus in gymnotiform electric fish: the accommodation of two behaviors in one nucleus. J Comp Neurol 276:113–131.

Keller CH, Kawasaki M, Heiligenberg W (1991) The control of pacemaker modulations for social communication in the weakly electric fish Sternopygus. J Comp Physiol A 169:441–450.

Lee BB, Mandl G, Stean JPB (1969) Micro-electrode tip position marking in nervous tissue: a new dye method. Electroencephalogr Clin Neurophysiol 27:610–613.

Liao D, Hessler NA, Malinow R (1995) Activation of postsynaptically silent synapses during pairing-induced LTP in CA1 region of hippocampal slice. Nature 375:400–404.

Lissman HW (1958) On the function and evolution of electric organs in fish. J Exp Biol 35:156–191.

Llinás R, Nicholson C (1974) Analysis of field potentials in the central nervous system. In: Handbook of electroencephalography and clinical neurophysiology, Vol. 2B (Stevens CF, ed), pp 61–83. Amsterdam: Elsevier.

Lorenzo D, Silva AC, Borde M, Macadar O (2001) Electrogeneration in South American weakly electric fish. In: Sensory biology of jawed fishes: new insights (Kapoor BG, Hara TJ, eds), pp 121–160. New Delhi: Oxford & IBH Publishing Co. Pvt. Ltd.

Nowak L, Bregestovski P, Ascher P, Herbert A, Prochiantz A (1984) Magnesium gates glutamate-activated channels in mouse central neurones. Nature 307:462–465.

Spiro JE (1997) Differential activation of glutamate receptor subtypes on a single class of cells enables a neural oscillator to produce distinct behaviors. J Neurophysiol 78:835–847.

Szabo T (1957) Un noyau particulier dans la formation réticulée bulbaire de quatre poissons électriques appartenant à la famille des Gymnotidae. C R Acad Sci (B) (Paris) 244:1957–1959.

Trujillo-Cenóz O, Lorenzo D, Bertolotto C (1993) Identification of neuronal types in the medullary electromotor nucleus of Gymnotus carapo. J Comp Physiol A 173:750.

Waldeck RF, Pereda A, Faber DS (2000) Properties and plasticity of paired-pulse depression at a central synapse. J Neurosci 20:5312–5320.

Wolszon LR, Pereda A, Faber DS (1997) A fast synaptic potential mediated by NMDA and Non-NMDA receptors. J Neurophysiol 78:2693–2706.

*(Accepted 14 February 2006)*
*(Available online 23 March 2006)*